Journal of Materials Chemistry

Cite this: J. Mater. Chem., 2012, 22, 5304

www.rsc.org/materials

COMMUNICATION

Highly porous gallium oxide with a high CO_2 affinity for the photocatalytic conversion of carbon dioxide into methane†

Hang-ah Park, Jung Hoon Choi, Kyung Min Choi, Dong Ki Lee and Jeung Ku Kang*

Received 17th January 2012, Accepted 3rd February 2012
DOI: 10.1039/c2jm30337j

Highly porous gallium oxide was synthesized by reconstructing its surface and body with mesopores and macropores. For the first time, the efficient photocatalytic conversion of CO_2 into a high energy carrier, CH_4, using the porous gallium oxide was realized without any co-particle or sacrificial reagent. The enhanced photocatalytic activity is mainly attributed to the 300% higher CO_2 adsorption capacity, as well as the 200% increased surface area, compared to the bulk nanoparticles. Furthermore, we propose the new reaction pathway based on the result that the carbon dioxide was converted directly into methane without going through carbon monoxide intermediates.

Due to the fact that the earth's current primary energy source is obtained through the combustion of fossil fuels, resulting in pollution and a climate change, the idea of artificial photosynthesis that uses carbon dioxide (CO_2) to produce hydrocarbon fuels would offer an alternative durable source of energy.[1–5] Among these hydrocarbon fuels, a promising candidate fuel is methane (CH_4), since it carries a high amount of energy per mass (55.7 kJ g^{-1}). In order to convert CO_2 into CH_4, it is important to develop a novel photocatalyst that uses solar energy and has a high affinity for CO_2.[6–8]

Grimes *et al.*[9] studied a photocatalytic conversion of CO_2 using TiO_2 nanotubes, enabling charge carriers to readily reach surface species. Meanwhile, the photoactivity on the titania system was limited by its insufficient reduction potential[5] and high recombination rate of photo-generated electron–hole pairs.[10,11] Therefore, new hetero-structures combining with noble metals[12] such as Pt[13] and Ru[14] have been suggested to be used for the separation of electron–hole pairs, but there is a problem that novel metals are expensive. However, metal oxide photocatalysts with d^{10} configurations (In^{3+}, Ga^{3+}, Ge^{4+}, Sn^{4+}, Sb^{5+})[15,16] are of great attention because hybridization between the s and p orbital of metals in the conduction band could enhance the mobility of photogenerated electrons, thus, producing high photocatalytic activity.[17] Among them, gallium oxide (Ga_2O_3) is a promising CO_2 reduction photocatalyst due to its high reduction potential for CO_2.[18–21] Tanaka *et al.*[20] carried out the photoreduction of CO_2 using H_2 as a reductant over the bulk crystal of β-Ga_2O_3, but found that it gave only CO as the product. Consequently, the further breakthrough on gallium oxide for the conversion of CO_2 into CH_4 has remained unsolved.

Herein, we report a novel porous gallium oxide with meso-pores and macropores. The small amount of photocatalytic reaction sites, which is the biggest problem[22] with working with gallium oxide, was solved by reconstructing its surface and body with mesopores and macropores, combining the template method with hydrolysis of gallium nitrate. The synthetic procedures of the new porous Ga_2O_3 and its CO_2 conversion processes are illustrated in Scheme 1. The efficient photocatalytic conversion of CO_2 into CH_4 was realized using the porous Ga_2O_3 without any co-particle or sacrificial reagent.

The field emission scanning electron microscopy (FESEM) image in Fig. 1(a) shows that porous Ga_2O_3 is rod-shaped and is monodispersed uniformly throughout the surface (see ESI†, Fig. S1†). Also, the cross-section SEM image in Fig. 1(b) and the transmission electron microscopy (TEM) image in Fig. 1(c) uncover the clear existence of inner and transmitted pores. In addition, the high resolution (HR) TEM image in Fig. 1(d) demonstrates the presence of mesopores below 5 nm in size and the X-ray diffraction pattern

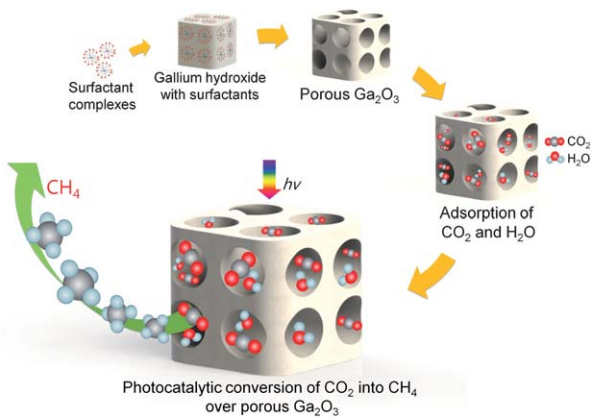

Scheme 1 Schematic diagram of the synthesis of porous Ga_2O_3 with mesopores and macropores, and the photocatalytic reaction process. Gallium hydroxide with surfactants was synthesized and then annealed to remove templates to form a porous Ga_2O_3 structure. CO_2 and H_2O were allowed to be adsorbed in pores and surface of the porous Ga_2O_3, and after light irradiation, CH_4 was generated over porous Ga_2O_3.

Graduate school of EEWS and Materials Science and Engineering, KAIST, 335 Gwahangno, Yuseong-gu, Daejeon 305-701, Republic of Korea. E-mail: jeungku@kaist.ac.kr

† Electronic supplementary information (ESI) available. See DOI: 10.1039/c2jm30337j

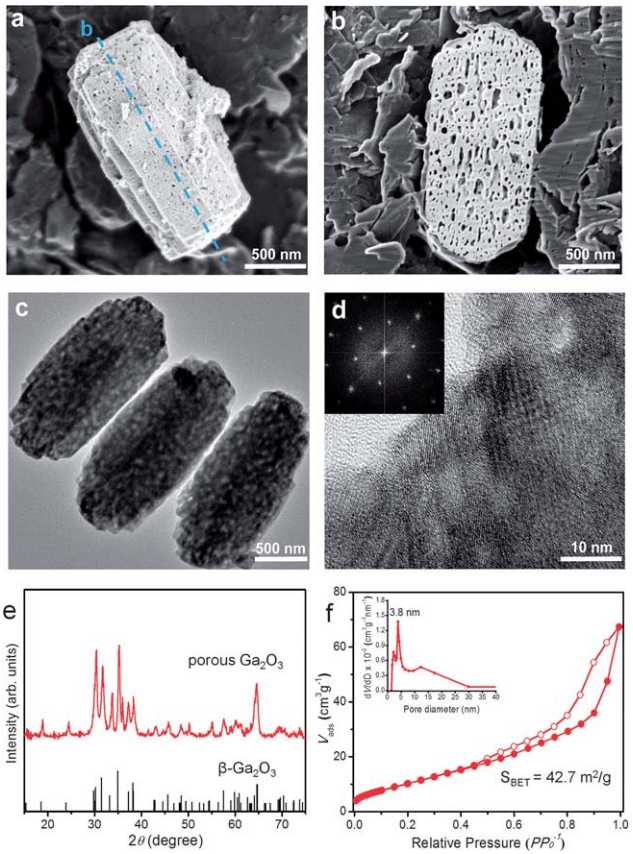

Fig. 1 Particle morphology, inner pores, and crystal structure of the synthesized Ga_2O_3. FESEM images of porous Ga_2O_3 with (a) top view and (b) vertical cross-sectional images fractured by the ion beam. (c) TEM image and (d) HRTEM with FFT images (inset). (e) XRD patterns of porous Ga_2O_3 particles on a monoclinic β-Ga_2O_3 phase (JCPDS 87-1901). (f) Nitrogen adsorption (filled symbol)–desorption (open symbol) isotherm and pore size distribution (inset) of the porous Ga_2O_3.

proves that porous Ga_2O_3 is crystalline. Fig. 1(e) shows that crystalline porous Ga_2O_3 that calcined at 873 K is in a monoclinic β-phase (JCPDS 87-1901), and ESI† Fig. S2† unveils that the templates used to make pore structures were completely removed. Fig. 1(f) shows the nitrogen adsorption–desorption isotherm on porous Ga_2O_3. The surface area from the N_2 isotherm using the Brunauer–Emmett–Teller (BET) model[23] ($P/P_0 = 0.05$ to 0.3) for porous Ga_2O_3 is 42.7 m^2 g^{-1}. The pore size distribution is estimated by the desorption isotherm, using the Barrett, Joyner, and Halenda (BJH) method.[24] The average mesopore size for the porous Ga_2O_3 is 3.8 nm, with a narrow distribution. Several ranges of mesopores were detected.

Fig. 2(a) shows the measured photocatalytic activity for the conversion of CO_2 into CH_4 over 50 mg of porous Ga_2O_3 as a function of time in the presence of CO_2 and H_2O vapor under photoirradiation. In the absence of photoirradiation, CH_4 was not detected in the gas phase. After light irradiation, CO_2 was converted into CH_4 by porous Ga_2O_3 photocatalysts, indicating a linear increase with time. The recycle reaction was also carried out after the evacuation of gases in the reactor and setting up to the initial photoreaction conditions. The evolution rate in this recycle reaction was unveiled to be restored to that of the original reaction. Fig. 2(b)

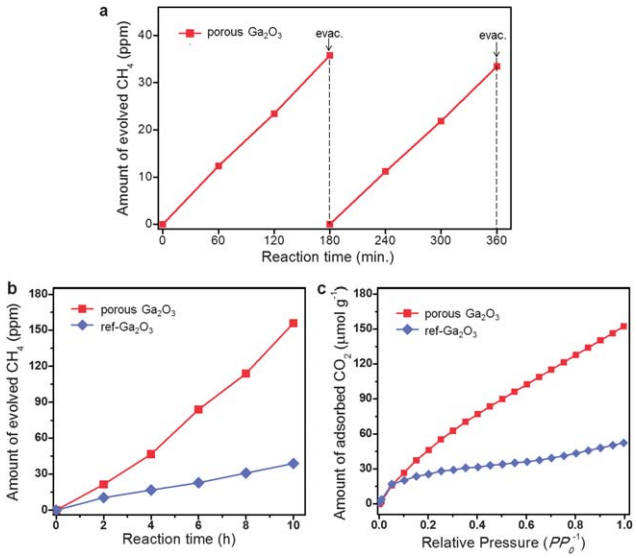

Fig. 2 (a) Measured recycles of photocatalytic activity of the conversion of CO_2 to CH_4 over 50 mg of porous Ga_2O_3, after the evacuation and purging of CO_2. (b) Continuous photocatalytic activity on evolved methane for 10 hours over 50 mg of porous Ga_2O_3 and ref-Ga_2O_3 samples. (c) CO_2 adsorption capacities of porous Ga_2O_3 and ref-Ga_2O_3 samples under ambient conditions.

illustrates the amount of CH_4 that has evolved from CO_2 over 50 mg of porous Ga_2O_3. The nanoparticles of β-Ga_2O_3 which is commercially available (ref-Ga_2O_3) were used as a reference sample. The ref-Ga_2O_3, with a relatively small BET surface area of 20.49 m^2 g^{-1} (see ESI† Fig. S3†), is in the same monoclinic β-phase as that of porous Ga_2O_3. Also, the UV-vis diffuse spectra of the porous Ga_2O_3 and the ref-Ga_2O_3 samples show their absorption edges at around 280 nm, as is evident in ESI† Fig. S4†. In this reaction, a large amount of CH_4 (2.09 μmol g^{-1}, 156 ppm) was produced through the CO_2 photocatalytic conversion over porous Ga_2O_3 particles, while ref-Ga_2O_3 produced smaller amounts of CH_4. In order to find the critical factor for the enhanced photo-catalytic activity, the volumetric CO_2 adsorption measurement was also carried out under ambient conditions. Fig. 2(c) shows the porous Ga_2O_3 has an adsorption capacity 300% higher than ref-Ga_2O_3. Generally, the photocatalytic reaction occurs on the surface of a photocatalyst that can function as a reactive site.[17,25] As seen in Fig. 1(f), porous Ga_2O_3 has a surface area that is larger than 200% of ref-Ga_2O_3. This means that a larger surface area provided more photocatalytic conversion sites. In addition, the porous Ga_2O_3 allowed CO_2 to be adsorbed with 3 times more capacity than that of ref-Ga_2O_3 at room temperature under one bar condition. Thus, it could be deduced that the higher CO_2 uptake capacity contributes to the high conversion rate of CO_2 into CH_4 by allowing more reactant CO_2 molecules to be adsorbed on the reactive surface.

Furthermore, it is noteworthy that the mesoporous channels of our synthesized Ga_2O_3 possess the advantage to promote the separation of electron–hole pairs. Charge carriers generated inside of the porous Ga_2O_3 could diffuse to the nearby mesopores where the gas molecules adsorbed, and convert CO_2 with the reactant molecules at the solid–gas interface for production of CH_4. In addition to mesopores, macropores are also significant for the photocatalytic reaction.[26] Cheng and co-workers[27] have reported that macroporous structures

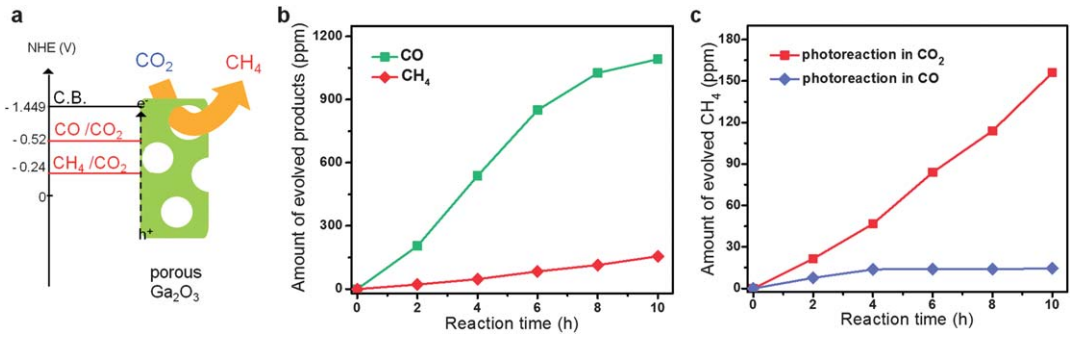

Fig. 3 (a) Energy band position of Ga_2O_3 and the redox potential of CO_2 at pH = 7, with respect to NHE. (b) The amount of the evolved products, CO and CH_4, in the same photocatalytic reaction of the CO_2 reduction. (c) Photocatalytic activity from different atmospheres; amount of evolved CH_4 in CO_2 (red line) and CO (blue line). Other conditions are similar to those of previous experiments.

with mesopores enhance the photocatalytic activity of the titania system because the macropores act as the channels for light-penetration and gas-diffusion. Consequently, the enhanced photocatalytic conversion of CO_2 into CH_4 is attributed to the unique porous Ga_2O_3 structure with mesopores and macropores.

The reason why Ga_2O_3 converts CO_2 into CH_4 in the presence of H_2O using solar energy can be explained based on the flat band positions of Ga_2O_3 as well as the redox potentials for water and CO_2 at pH = 7, with respect to NHE (normal hydrogen electrode). The schematic diagram is shown in Fig. 3(a). Ga_2O_3 has a good reduction potential for the photocatalytic conversion of CO_2 into CH_4. When Ga_2O_3 absorbs light, the electron in the valence band is excited to the conduction band, and it would transfer to the surface of the Ga_2O_3 where it reacts with CO_2 or intermediate molecules adsorbed. Meanwhile, a hole meets a water molecule to produce a proton (H^+). Then, photoexcited electrons and protons contribute to conversion of CO_2 into CH_4, where the required energy for CH_4 production is −0.24 eV (*vs.* NHE). The edge of the conduction band potential for Ga_2O_3 lies at −1.449 eV (*vs.* NHE), which means that Ga_2O_3 has sufficient reduction energy to produce CH_4 from CO_2 under light.

In order to determine a more detailed reaction mechanism, we measured carbon monoxide (CO) from the same reaction of the original test. Fig. 3(b) shows the photogenerated carbon monoxide and methane from carbon dioxide over 50 mg of porous Ga_2O_3. After light irradiation, a large amount of CO (14.63 μmol g^{-1}, 1092 ppm) was produced through the photo-catalytic conversion of CO_2. The required energy for carbon monoxide production is −0.52 eV (*vs.* NHE), and the edge of the conduction band potential for Ga_2O_3 is sufficient to produce CO from CO_2. The evolved CO amount is seven times higher than CH_4, which means carbon dioxide is more likely to reduce into carbon monoxide than methane.

Since a large amount of CO molecules as well as CH_4 was produced in the photoreaction, we conducted a further experiment on the photocatalytic reduction of CO into CH_4 in order to determine whether CO_2 can be reduced into CH_4 *via* CO or not. The experiment was carried out in CO gas, instead of CO_2, but otherwise under the same conditions as the previous photo-reaction. Fig. 3(c) illustrates that there was a negligible amount of CH_4 produced when CO was converted to CH_4, as compared to the amount of CH_4 that was produced when CO_2 was converted into CH_4. As this result shows, the CO_2 molecules were converted into CH_4 not *via* CO intermediates, because carbon monoxide is hardly reduced into methane in the gallium oxide system. Therefore, in order to efficiently convert carbon dioxide into methane, it is pivotal to control reaction pathways of selective methane production. On the basis of these photo-catalytic reaction results, the carbon dioxide conversion mechanism in the gallium oxide system could be postulated as follows:

$$Ga_2O_3 + h\nu \rightarrow h^+ + e^- \quad (1)$$

$$H_2O + h^+ \rightarrow H^+ + OH^{\cdot} \quad (2)$$

$$CO_2 + 8e^- + 8H^+ \rightarrow CH_4 + 2H_2O \quad (3)$$

$$CO_2 + 2e^- + 2H^+ \rightarrow CO + H_2O \quad (4)$$

$$CO + 6e^- + 6H^+ \nrightarrow CH_4 + H_2O \quad (5)$$

In order to evaluate the photocatalytic efficiency, the quantum yield is calculated, which is defined by eqn (6) (ref. 15)

$$\text{Quantum yield } (\%) = \frac{\text{Number of reacted electrons}}{\text{Number of incident photons}} \times 100\% = \frac{8 \times \text{Number of evolved } CH_4 \text{ molecules}}{\text{Number of incident photons}} \times 100\% \quad (6)$$

The quantum yield of CH_4 evolution using 50 mg porous Ga_2O_3 for 1 h is calculated to be 3.993%.

In conclusion, novel porous Ga_2O_3 which embodied mesopores and macropores in its surface and body was successfully synthesized by hydrolysis combined with the template method. The photocatalytic conversion of CO_2 into CH_4 using the porous gallium oxide was realized for the first time with about 400% higher conversion rate than that of ref-Ga_2O_3. The enhanced photocatalytic activity is attributed to the CO_2 adsorption capacity higher by about 300%, resulting from the unique meso- and macropore structure, as well as the increased reactive sites by about 200% than those of ref-Ga_2O_3. Moreover, CO_2 was converted directly into methane not *via* CO intermediates, which indicates the CO_2 conversion efficiency can be improved by controlling reaction pathways or combining other photocatalysts converting CO into CH_4. Consequently, these results provide the potential of the porous gallium oxide material, and the new clue to enable the efficient conversion of CO_2 into hydrocarbon fuels *via* artificial photosynthesis.

Methods

Preparation of porous gallium oxide

50 mg TTAB was dissolved in a solution composed of 25 ml of H_2O with 1.5 ml NH_4OH at 343 K, and then 0.01 ml of 1-dodecanethiol was added into the solution. The mixture was stirred for 30 minutes at 343 K. In the meantime, 1 g of gallium nitrate hydrate ($Ga(NO_3)_3 \cdot xH_2O$) was dissolved in 200 ml of ethanol (50 vol%). Next, the mixture containing the surfactant was added to the ethanolic gallium nitrate solution, and stirred for 2 hours at 343 K. The resulting precipitate was filtered under vacuum, washed with distilled water, and dried under reduced pressure overnight. Lastly, the obtained solid was calcined at 873 K for 6 hours to remove organics and surfactants, and to form the β-phase Ga_2O_3.

Characterization

Field emission scanning electron microscopy (FESEM) (JSM7600F) and Cs-corrected scanning transmission electron microscopy (JEM-ARM200F) have been used to produce the structural information. In addition, the crystallinity of the Ga_2O_3 samples was determined by the powder X-ray diffraction pattern (XRD) (D/MAX-III C, 3 kW), and the gas adsorption–desorption measurements for N_2 and CO_2 were carried out on a Quantachrome Autosorb-6 system by the volumetric method.

Evaluation of photocatalytic properties

The photocatalytic experiments were carried out in a closed chamber system with gas inlet and outlet valves, a quartz window top, a septum-attached port, and a thermocouple connected to the chamber. Fifty mg of Ga_2O_3 was loaded on a glass holder in the bottom of a reactor (dead volume: 15.74 ml). The chamber was purged with CO_2, and distilled water (3 mmol) was injected into the chamber and evaporated. Next, the sample was irradiated through the top quartz window using a 300 W Xe lamp equipped with a cooling system and an IR cutting filter with the light intensity of 500 mW cm^{-2}. Two hundred μl of the gas was periodically captured from the reactor using the gas tight syringe with the volume reproducible adaptor. The reaction was analyzed using the gas chromatograph (Agilent Technologies 7890A), with the thermal conductivity detector (TCD) equipped with a packed column and a 5 Å molecular sieve, and argon was used as a carrier gas. Product gases were calibrated with a standard mixture gas and determined by the retention time.

Acknowledgements

This work was supported by the Korea Center for Artificial Photosynthesis (KCAP) funded by the Ministry of Education, Science, and Technology (NRF-2011-C1AAA001-2011-00302 78), by the WCU (World Class University) program (R-31-2008-000-10055-0), by the grants from National Research Foundation (NRF-R0A-2007-000-20029-0, NRF-2011-0028737, NRF-2009-0094039, and NRF-2010-0007692) and by the Hydrogen Energy R&D Center.

Notes and references

1 J. R. McKone, E. L. Warren, M. J. Bierman, S. W. Boettcher, B. S. Brunschwig, N. S. Lewis and H. B. Gray, *Energy Environ. Sci.*, 2011, **4**, 3573.
2 M. G. Walter, E. L. Warren, J. R. McKone, S. W. Boettcher, Q. Mi, E. A. Santori and N. S. Lewis, *Chem. Rev.*, 2010, **110**, 6446.
3 Y. Lee, J. H. Choi, H. J. Jeon, K. M. Choi, J. W. Lee and J. K. Kang, *Energy Environ. Sci.*, 2011, **4**, 914.
4 S. C. Roy, O. K. Varghese, M. Paulose and C. A. Grimes, *ACS Nano*, 2010, **4**, 1259.
5 A. F. Collings and C. Critchley, *Artificial Photosynthesis*, Wiley-VCH, Weinheim, 2005, pp. 13.
6 X. Wang, K. Maeda, A. Thomas, K. Takanabe, G. Xin, J. M. Carlsson, K. Domen and M. Antonietti, *Nat. Mater.*, 2009, **8**, 76.
7 V. P. Indrakanti, J. D. Kubickib and H. H. Schobert, *Energy Environ. Sci.*, 2009, **2**, 745.
8 T. Inoue, A. Fujishima, S. Konishi and K. Honda, *Nature*, 1979, **277**, 637.
9 O. K. Varghese, M. Paulose, T. J. LaTempa and C. A. Grimes, *Nano Lett.*, 2009, **9**, 731.
10 M. R. Hoffmann, S. T. Martin, W. Choi and D. W. Bahnemann, *Chem. Rev.*, 1995, **95**, 69.
11 A. J. Cowan, J. Tang, W. Leng, J. R. Durrant and D. R. Klug, *J. Phys. Chem.*, 2010, **114**, 4208.
12 Y. L. Chen, D. Z. Li, X. C. Wang, X. X. Wng and X. Z. Fu, *Chem. Commun.*, 2004, 2304.
13 Q. H. Zhang, W. D. Han, Y. J. Hong and J. G. Yu, *Catal. Today*, 2009, **128**, 335.
14 N. Sasirekha, S. J. S. Basha and K. Shanthi, *Appl. Catal., B*, 2006, **62**, 169.
15 X. Chen, S. Shen, L. Guo and S. S. Mao, *Chem. Rev.*, 2010, **110**, 6503.
16 Y. Inoue, *Energy Environ. Sci.*, 2009, **2**, 364.
17 K. Maeda, K. Teramura, N. Saito, Y. Inoue, H. Kobayashi and K. Domen, *Pure Appl. Chem.*, 2006, **78**, 2267.
18 Y. Pan, C. Liu, D. Mei and Q. Ge, *Langmuir*, 2010, **26**, 5551.
19 M. Calatayud, S. E. Collins, M. A. Baltana and A. L. Bonivardi, *Phys. Chem. Chem. Phys.*, 2009, **11**, 1397.
20 H. Tsuneoka, K. Teramura, T. Shishido and T. Tanaka, *J. Phys. Chem. C*, 2010, **114**, 8892.
21 S. E. Collins, M. A. Baltanas and A. L. Bonivardi, *J. Phys. Chem. B*, 2006, **110**, 5498.
22 C. Tagusagawa, A. Takagaki, A. Iguchi, K. Takanabe, J. N. Kondo, K. Ebitani, S. Hayashi, T. Tatsumi and K. Domen, *Angew. Chem., Int. Ed.*, 2010, **49**, 1128.
23 S. Brunauer, P. H. Emmett and E. Teller, *J. Am. Chem. Soc.*, 1938, **60**, 309.
24 E. P. Barrett, L. G. Joyner and P. P. Halenda, *J. Am. Chem. Soc.*, 1951, **73**, 373.
25 Y. Hou, X. Wang, L. Wu, Z. Ding and X. Fu, *Environ. Sci. Technol.*, 2006, **40**, 5799.
26 J. Liu, M. Li, J. Wang, Y. Song, L. Jiang, T. Murakami and A. Fujishima, *Environ. Sci. Technol.*, 2009, **43**, 9425.
27 J. Yu, Y. Su and B. Cheng, *Adv. Funct. Mater.*, 2007, **17**, 1984.